Journal of Biomedical Optics

SPIEDigitalLibrary.org/jbo

Sensing dynamic cytoplasm refractive index changes of adherent cells with quantitative phase microscopy using incorporated microspheres as optical probes

Sabine Przibilla
Sebastian Dartmann
Angelika Vollmer
Steffi Ketelhut
Burkhard Greve
Gert von Bally
Björn Kemper

SPIE

Sensing dynamic cytoplasm refractive index changes of adherent cells with quantitative phase microscopy using incorporated microspheres as optical probes

Sabine Przibilla,[a] Sebastian Dartmann,[a] Angelika Vollmer,[a] Steffi Ketelhut,[a] Burkhard Greve,[b] Gert von Bally,[a] and Björn Kemper[a]
[a]University of Muenster, Center for Biomedical Optics and Photonics, Robert-Koch-Str. 45, D-48149 Muenster, Germany
[b]University Hospital Muenster, Department of Radiotherapy, Albert-Schweitzer Campus 1, D-48149 Muenster, Germany

Abstract. The intracellular refractive index is an important parameter that describes the optical density of the cytoplasm and the concentration of the intracellular solutes. The refractive index of adherently grown cells is difficult to access. We present a method in which silica microspheres in living cells are used to determine the cytoplasm refractive index with quantitative phase microscopy. The reliability of our approach for refractive index retrieval is shown by data from a comparative study on osmotically stimulated adherent and suspended human pancreatic tumor cells. Results from adherent human fibro sarcoma cells demonstrate the capability of the method for sensing of dynamic refractive index changes and its usage with microfluidics. [DOI: 10.1117/1.JBO.17.9.097001]

Keywords: digital holographic microscopy; quantitative phase imaging; cellular refractive index; live cell imaging; microspheres.

Paper 12263 received Apr. 28, 2012; revised manuscript received Jul. 14, 2012; accepted for publication Jul. 30, 2012; published online Sep. 6, 2012.

1 Introduction

Quantitative phase microscopy enables high-resolution inspection of reflective surfaces and label-free, minimally invasive, live cell analysis. Various different methods have been developed,[1–16] however, in quantitative phase microscopy, the optical path length delay, which is caused by a semitransparent specimen, is influenced by the sample thickness, the refractive index of the sample, and the refractive index of the surrounding medium. For this reason, in quantitative phase imaging-based live cell analysis, the intra cellular refractive index represents a very important parameter.

On one hand, knowledge about the cellular refractive index is required for reliable investigations on the cell morphology.[7,17,18] On the other hand, the refractive index and its spatial distribution is related to the density of cell organelles and the cytoplasm[19] and dynamic changes of intracellular solute concentrations due to osmotic stimulation[20] or growth processes,[21] and thus represents also a versatile parameter that can be utilized for label-free cell tomography.[22–24]

Early experiments to determine the average refractive index of multiple cells were reported in 1957 by Barer et al.[25] Later, confocal microscopy[26] as well as microfluidic chip based devices[27] were utilized to record data about the cellular refractive index. As already mentioned, the cellular refractive index is very important in quantitative phase microscopy. For this reason, also several concepts for refractive index determination of living single cells that are based on these methods have been proposed. In Ref. 28, the refractive index of red blood cells is determined by defocusing microscopy. Rappaz et al.[20] report a digital holographic microscopy (DHM)-based procedure for the retrieval of the integral refractive index of neurons in which two cell culture media with slightly different refractive indices are applied. In Ref. 17, a glass cover was pressed onto cells to ensure uniform cell thickness, and the integral cellular refractive index of adherent cancer cells was determined with DHM using phase changes due to air inclusions as a reference. Lue et al.[29] proposed a similar method based on Hilbert phase microscopy in which microfluidic equipment was used to ensure a constant cell thickness. In Refs. 30–32, digital holographic phase contrast images of spherical cells in suspension were recorded, and the radius as well as integral refractive index were decoupled by fitting the relationship between cell thickness and phase distribution to measured phase data. In Ref. 19, the hemoglobin concentration of red blood cells was analyzed by a spectroscopic approach in which data from separate quantitative phase imaging-based refractive index measurements on known hemoglobin solutions were considered. In Ref. 18, the principle in Ref. 19 was modified for single shot measurements by using a color sensitive charge coupled device sensor. Robles et al.[33] analyzed dispersion effects in red blood cells by nonlinear phase spectroscopy. In Ref. 34, the refractive index and the cellular thickness were decoupled by DHM utilizing a two-wavelength method in combination with an enhanced dispersion of the perfusion medium achieved by an extracellular dye. In Refs. 35 and 36, a DHM-based refractive index tomography of cellular samples was performed by recording multiple phase contrast images of a rotated sample. Similar results were obtained by Choi et al.[23] with Fourier phase microscopy, and by Lauer[22] and Debailleul et al.[24] with Mach-Zehnder interferometer-based diffractive microscopy by illumination of the sample in transmission from different directions. However,

Address all correspondence to: Björn Kemper, University of Muenster, Center for Biomedical Optics and Photonics, Robert-Koch-Str. 45, D-48149 Muenster, Germany; Tel: +49 251 83 52479; Fax: +49 251 83 58536; E-mail: bkemper@uni-muenster.de

0091-3286/2012/$25.00 © 2012 SPIE

the reliable determination of the cellular refractive index, in particular of adherently grown cells, still remains a challenge.

Here, we explore a method to determine the integral refractive index of the cytoplasm of living cells by using incorporated silica microspheres and quantitative phase microscopy based on DHM. The main advantages of this approach are that the method can be used with irregularly shaped adherent cells and simple setups for quantitative phase imaging; for example, no tilts of the object illumination or imaging with several wavelengths from different light sources are required. Furthermore, the method prospects to be used with several existing approaches for quantitative phase microscopy. As many cells incorporate particles due to phagocytic behavior,[37] the method may be used for the analysis of a variety of different cell types. It will also be shown that quantitative phase imaging represents a versatile label-free method to verify if semi-transparent microparticles are internalized by a living cellular specimen, and to verify if the proposed principle for cell refractive index determination is capable for usage with microfluidics.

2 Materials and Methods

2.1 *Cells*

Human pancreatic ductal adenocarcinoma cells (PaTu 8988 T)[38] used in this study were obtained from the German Collection of Microorganisms and Cell Cultures (DSMZ, Braunschweig, Germany). The cells were cultured in dulbecco's modified eagle's medium (DMEM) supplemented with 5% fetal calf serum, 5% horse serum, and 2-mM L-glutamine under standard cell culture conditions (37°C and 10% CO_2).

For quantitative DHM phase imaging of adherent cells the cells were seeded in Petri dishes (μ-dish, ibidi GmbH, Munich, Germany). For quantitative phase analysis of suspended cells, the cells were trypsinized and investigated in Petri dishes with an uncoated "hydrophobic" bottom (μ-dishes, ibidi GmbH, Munich, Germany) to prevent cell adherence during the experiments. In order to manipulate the cellular refractive index, the cells were observed in diluted cell culture medium with decreased osmolality. Therefore, deionized water was added to the initial Hepes buffered cell culture medium.

Human fibro sarcoma cells HT-1080[39] were cultured in DMEM supplemented with 10% fetal calf serum and 2-mM L-glutamine at 37°C with 10% CO_2. These cells were observed after adherence in microfluidic channels (μ-Slides, ibidi GmbH, Munich, Germany). To induce a decrease and increase of the cellular refractive index the initial Hepes buffered cell culture medium with an osmolality of 320 mOsmol/kg was replaced by medium that was diluted with deionized water to 160 mOsmol/kg. An automated pump system (ibidi pump system, ibidi GmbH, Munich, Germany) was applied to achieve a reproducible exchange of the medium.

2.2 *Incubation of the Cells with Microparticles*

The cells were incubated with uncoated silica (SiO_2) microspheres (Microparticle GmbH, Berlin, Germany, diameter ≈ 3.44 μm). Uncoated silica microspheres were chosen due to the non-toxicity of the material. The refractive index of the spheres amounts to about 1.43 (see also Sec. 3.1) and is in combination with the diameter of ≈3.44 μm particularly suitable for usage with DHM as in aqueous solutions and living cells diffraction

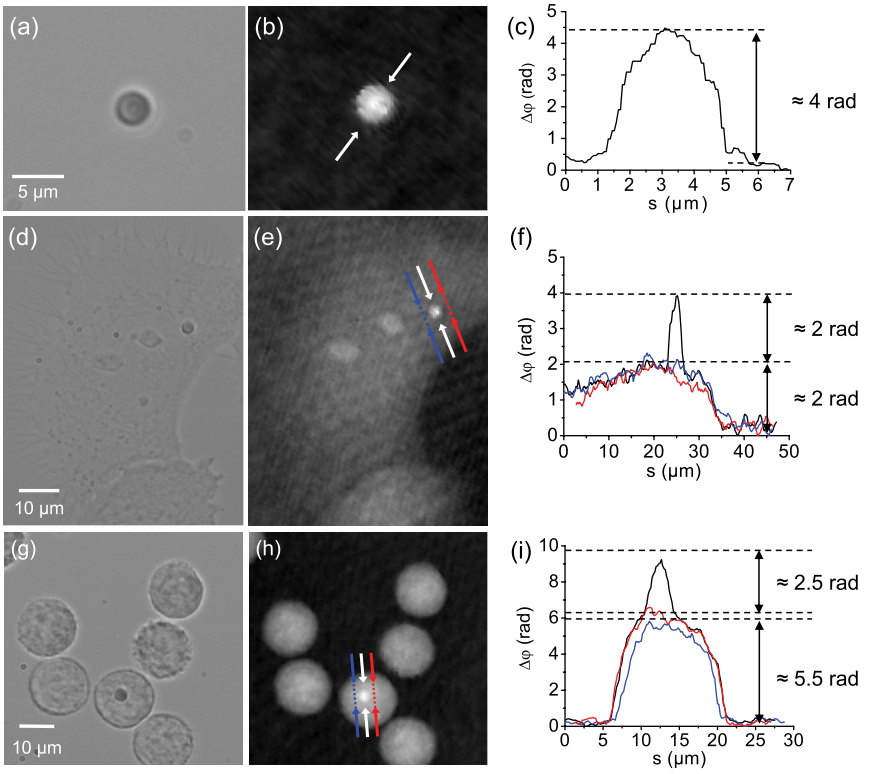

Fig. 1 Verification of the internalization of silica microspheres in adherent and suspended PaTu 8988 T cells by quantitative digital holographic microscopy (DHM) phase imaging. (a), (d), (g) white light images of a SiO_2 microsphere, an adherent cell with an incorporated microsphere and a suspended cell with an incorporated microsphere. (b), (e), (h) quantitative phase images corresponding to (a), (d) and (g), respectively. (c), (d), (i) cross-sections through the phase contrast images in (b), (e) and (h), respectively, through and near the microspheres [see arrows in (b), (e) and (h)].

patterns at the particles borders are minimized [for illustration see Fig. 1(a) and 1(b)]. The diameter of the spheres was also chosen as a minimum particle size, and is required for imaging with the used DHM setups and the utilized microscope lenses (see Sec. 2.3) to achieve a sufficient number of image pixels and an adequate quantitative phase contrast to the surrounding medium suitable for the fitting procedure described in Sec. 2.4.

Prior to incubation with the cells, the particles were autoclaved ($T > 121$°C, $P = 2$ bar). Then, during the cultivation in cell culture flasks, PaTu 8988 T and HT-1080 cells were incubated for 48 h with a concentration of about five particles per cell in DMEM (see Sec. 2.1). Afterwards, the cells were detached and seeded into the Petri dishes or the microfluidic channels used for observation with DHM. After incubation for additional 24 h with a concentration of five microspheres per cell, about 20% of the cells internalized at least a single microsphere. Prior to the DHM measurements, non-engulfed microspheres were removed by washing the sample twice with cell culture medium. For investigations on suspended cells, the cells were detached again. A 5-Brom-2-desoxyuridin (BrdU) assay,[40] which was performed with a flow cytometer (Cyflow space, Partec GmbH, Muenster, Germany), showed

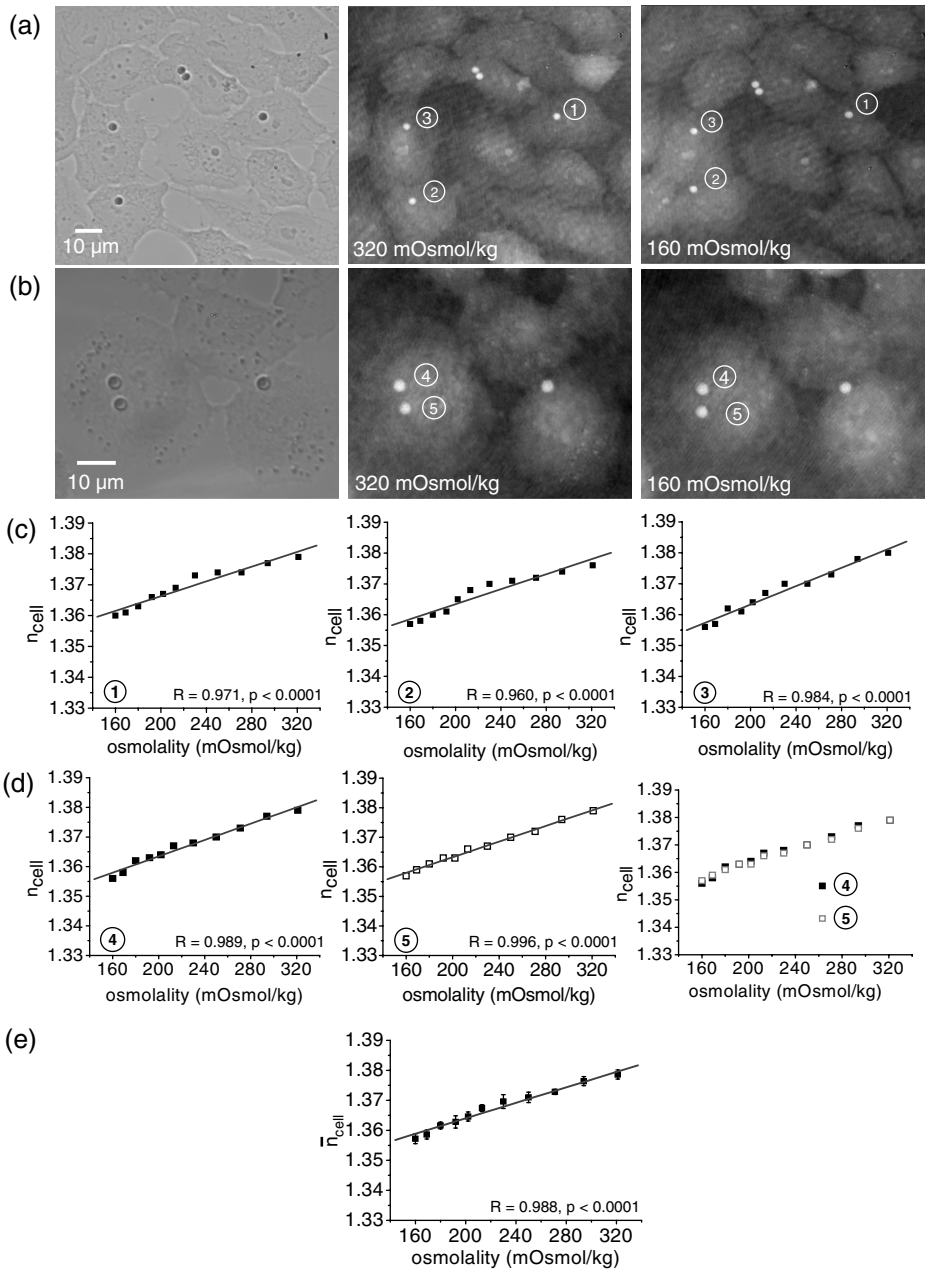

Fig. 2 Refractive index determination of the cytoplasm in osmotically stimulated adherent PaTu 8988 T cells. (a) using microspheres that were incorporated by three different cells; left: white light image, middle: quantitative digital holographic microscopy (DHM) phase image for 320 mOsmol/kg; right: quantitative DHM phase image for 160 mOsmol/kg. (b) using two microspheres within a single cell; left: white light image; middle: quantitative DHM phase image for 320 mOsmol/kg; right: quantitative DHM phase image for 160 mOsmol/kg. (c) n_{cell} versus osmolality detected with the microspheres denoted with (1), (2), (3) in (a). (d) left and middle panel: n_{cell} vs. osmolality detected with the microspheres denoted with (4), (5) in (b); right panel: data from microspheres (4) and (5) plotted in a single graph. (e) mean values $\bar{n}_{cell}$ versus osmolality obtained from the plots in (c) and (d). The solid lines in (c), (d), (e) correspond to linear fits (R: Pearson correlation coefficient, p: p-value).

no influence of the microparticles on cell proliferation. This correlates with the appearance of the cells in white light images and quantitative DHM phase images in which no morphologic alterations of the cells with internalized microspheres in comparison to control cells were observed [for illustration see Fig. 2(a) and 2(b)].

2.3 *Quantitative Phase Imaging with DHM*

PaTu 8988 T cells were observed with an inverted microscope (Zeiss Axio Observer A1, Carl Zeiss Micro Imaging GmbH, Goettingen, Germany) with an attached DHM module that is based on a principle which has been described elsewhere.[41] HT-1080 cells were investigated with a recently developed self-interference DHM setup[42] which was adapted to the same inverted microscope. For both setups the coherent light source was a frequency-doubled Nd: YAG laser (Compass 315M-100, Coherent, Luebeck, Germany, $\lambda = 532$ nm). Digital off-axis holograms and self-interference digital holograms of selected adherent and suspended cells were recorded with a charge-coupled device sensor (CCD, 1280×960 pixels, The imaging source DMK 41BF02, Bremen, Germany). For imaging, $20x$ and $40x$ microscope lenses (Zeiss LD Acroplan $20x/0.4$ Korr, Zeiss LD Plan-Neofluar, $40/0.6$ Korr) were used. All holograms were captured with exposure times below one millisecond to minimize influence of vibrations, movements of suspended cells, and flow of the cell culture medium. The numerical reconstruction of the quantitative DHM phase images from the digital holograms was performed subsequently by spatial phase shifting[4,17] in combination with numerical autofocusing.[43] All experiments in this study were performed at room temperature and normal atmosphere.

2.4 *Procedure for Determining the Cellular Refractive Index*

It is possible to determine the refractive index of spherical objects like suspended cells or microspheres in suspension from quantitative DHM phase images.[30,31] For a sharply focused mainly transparent specimens with a known homogeneously distributed refractive index n_s in a surrounding medium with refractive index n_{medium}, the relation between the thickness of the sample $d_s(x,y)$ and the induced optical path length change $\Delta\varphi_s$ to the surrounding medium is:

$$\Delta\varphi_s(x,y) = \frac{2\pi}{\lambda} d_s(x,y) \cdot (n_s - n_{\text{medium}}). \tag{1}$$

For suspended spherical cells or microspheres with radius R_s that are located at $x = x_0$, $y = y_0$, the thickness of the specimen $d_s(x,y)$ is:

$$d_s(x,y) = \begin{cases} 2 \cdot \sqrt{R_s^2 - (x-x_0)^2 - (y-y_0)^2} & \text{for } (x-x_0)^2 + (y-y_0)^2 \le R_s^2 \\ 0 & \text{for } (x-x_0)^2 + (y-y_0)^2 > R_s^2 \end{cases}. \tag{2}$$

Insertion of Eq. (1) in Eq. (2) yields:

$$\Delta\varphi_s(x,y) = \begin{cases} \frac{4\pi}{\lambda} \cdot \sqrt{R_s^2 - (x-x_0)^2 - (y-y_0)^2} \cdot (n_s - n_{\text{medium}}) & \text{for } (x-x_0)^2 + (y-y_0)^2 > R_s^2 \\ 0 & \text{for } (x-x_0)^2 + (y-y_0)^2 > R_s^2 \end{cases}. \tag{3}$$

To obtain the unknown parameters of interest n_s, (or n_{medium}) and R_s, Eq. (3) is fitted iteratively in two-dimensions to the experimentally obtained phase data.[30,31] Iterative two-dimensional fitting of Eq. (3) to phase data was performed in order to consider a maximum number of phase values for the refractive index and size determination of small specimens like the microspheres used in this study. In order to minimize the influence of diffraction, phase values close to the outer borders of the particles or cells in the image plane were excluded by application of an adequate threshold value.[30] For the retrieval of the refractive indices of suspended spherical particles (n_{part}) or cells (n_{cell}) with Eq. (3) for n_{medium}, the refractive index of the surrounding medium is used while $n_s := n_{\text{part}}$ (or $n_s := n_{\text{cell}}$) is determined by fitting. For the determination of the refractive index of adherent or suspended cells with incorporated particles, $n_s := n_{\text{part}}$ is used while $n_{\text{medium}} := n_{\text{cell}}$ is obtained by the fitting process.

2.5 *Characterization of the Osmolality and Refractive Index of Dilutions Used*

The osmolality of all dilutions in this study was determined by an osmometer (Osmomat 030, Gonotec GmbH, Berlin, Germany). The refractive indices of all media were measured by an Abbe refractometer (WYA-2W, Hinotek Ltd, Ningbo, China).

3 Results

3.1 *Characterization of the Microspheres*

From the manufacturer no precise information about the refractive index of the microspheres at the observation wave length of $\lambda = 532$ nm was available. Furthermore, adsorption of intracellular solutes may induce changes in the size and the integral refractive index of the particles. Thus, in a first experiment the radius and the refractive index of the microspheres were determined by quantitative DHM phase imaging in deionized water ($n_{\text{medium}} := 1.334$), in a solution with fetal calve serum (FCS, $n_{\text{medium}} := 1.335$) that includes various different proteins and in a phosphate buffered saline (PBS) solution with 10% bovine serum albumin (BSA, $n_{\text{medium}} := 1.339$) using the procedure described in Sec. 2.4. Table 1 shows the experimentally obtained mean values for the radius $R_s := R_{\text{part}}$ and the refractive indices $n_s := n_{\text{part}}$ of the microspheres.

The values for R_{part} slightly increase in the two protein solutions while within the measurement uncertainty no significant changes of the refractive indices are detected. The increase of the particle radius in the FCS and BSA solutions indicates

Table 1 Radius R_{part} and refractive index n_{part} of SiO_2 microspheres in different solutions (N: number of investigated microspheres, FCS: fetal calve serum, BSA: bovine serum albumin). The measurement uncertainty is quantified by the standard deviation from the mean value.

Solution	N	R_{part} (μm)	n_{part}
H_2O	75	1.74 ± 0.09	1.435 ± 0.006
FCS	104	1.78 ± 0.08	1.433 ± 0.005
PBS + 10% BSA	104	1.80 ± 0.07	1.436 ± 0.005

that for measurements within cells adsorption of intracellular solutes can be expected. However, this does not influence the particle refractive index within the statistical error range. Thus, for the refractive index determination experiments with microspheres in cells as reference in quantitative phase images that are described in Secs. 3.4 to 3.6, the mean value of all $N = 183$ measurements $[n_{part}(H_2O) + n_{part}(FCS) + n_{part}(BSA)]/3 = 1.435 \pm 0.005$ was used.

3.2 *Verification of Internalization of Microspheres by DHM Phase Contrast*

The incorporation of microspheres due to phagocytic behavior in adherent and suspended cells was checked by analysis of DHM phase images. Figure 1 depicts representative results. Figure 1(a) and 1(b) shows a white light image and a corresponding DHM phase contrast image of a microsphere in cell culture medium ($n_{medium} = 1.339$). A cross-section through the phase map along the white arrows in Fig. 1(b) is plotted in Fig. 1(c). Note that at the particle borders a slight phase decrease due to diffraction is observed. This justifies the application of a threshold value to the phase data prior the fitting procedure for refractive index determination that is described in Sec. 2.4. The maximum particle induced phase contrast amounts to ≈4 rad. Figure 1(d) shows a white light image of a living adherent PaTu 8988 T cell that contains a microsphere. In Fig. 1(f), three different cross-sections through the corresponding quantitative phase image of the cell [Fig. 1(e)] near and through the particle are plotted. The phase difference that is caused by the particle in addition to the cell induced phase change amounts to ≈2 rad [Fig. 1(f)]. This is significantly lower than the phase contrast of the pure particle in cell culture medium [see Fig. 1(c)]. Taking into account the result in Fig. 1(c), for microparticle adherence outside the cell a phase contrast difference of ≈4 rad in addition to the cell induced phase change would be expected. Figure 1(g) to 1(i) illustrates the verification of particle internalization in a suspended PaTu 8988 T cell. In correspondence to the results in Fig. 1(f), the phase contrast of the microsphere in the analyzed cell [white arrows in Fig. 1(h)] amounts to ≈2.5 rad [black line in Fig. 1(i)] which is lower than in cell culture medium.

The observed phase contrast decrease of the particles in cells is plausible and in agreement with Eq. (1) as the refractive index of the cytoplasm is higher than that of the cell culture medium. Note that in Fig. 1(e) to 1(i), within the measurement uncertainty, no influence of diffraction at the lateral borders of the microspheres is observed in the DHM quantitative phase images. This is also plausible as the refractive index difference between the internalized particles and the cytoplasm is lower than for the particle in cell culture medium. In conclusion, the results in Fig. 1 demonstrate the label-free verification of the internalization of microspheres in living adherent and suspended cells by DHM phase contrast.

3.3 *Cytoplasm Refractive Index Determination in Adherent Cells Using Microspheres*

In the next experimental step, the refractive index of adherent PaTu 8988 T cells was determined by using the internalized microspheres as reference in quantitative DHM phase images. In order to ensure that the whole microspheres were surrounded by the cytoplasm only engulfed particles with location near the nucleus were analyzed. Specimens near the outer cell borders were excluded as the cell thickness in this area is expected to be lower than the particle diameter.[17] First, the incorporation of three selected microspheres [indicated with 1, 2, and 3 in Fig. 2(a)] was verified as described in Sec. 3.3. Then, the osmolality of the cell culture medium was successively decreased in 10 steps from 320 mOsmol/kg to 160 mOsmol/kg. After each dilution step quantitative DHM phase images were generated and analyzed as described in Sec. 2.4.

Figure 2(a) shows a white light image and two representative quantitative DHM phase images of the cells for the initial and final osmolality. On the right panel of Fig. 2(a), cell swelling due to the dilution of the cell culture medium becomes visible. In Fig. 2(c), the intracellular refractive index determined with each particle is plotted versus the osmolality of the cell culture medium. The initial refractive index in isotonic cell culture medium for all three cells amounts to $n_{cell}(320\ \text{mOsmol/kg}) \approx 1.38$, while for the final refractive index values around $n_{cell}(160\ \text{mOsmol/kg}) \approx 1.36$ are detected. The comparison to a linear fit [see solid lines in Fig. 2(c)] illustrates a mainly proportional dependency (Pearson correlation coefficient $R \geq 0.960$, p-value <0.0001) between n_{cell} and the osmolality for all three microspheres.

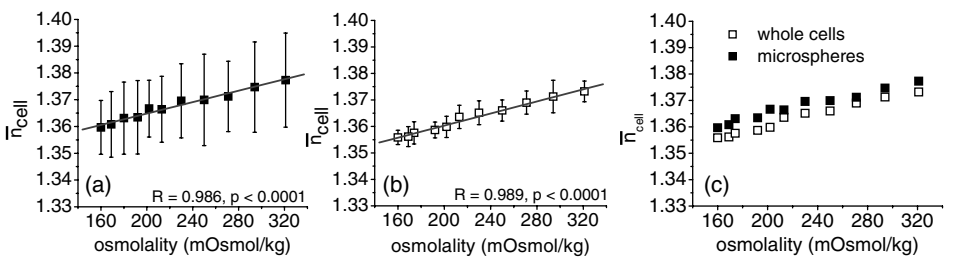

Fig. 3 Refractive index $\bar{n}_{cell}$ versus osmolality of osmotically stimulated suspended PaTu 8988 T cells. (a) Determined with incorporated microspheres as a reference. (b) Obtained by analyzing whole spherical cells in cell culture medium. (c) Results from (a) and (b) plotted in a single graph (R: Pearson correlation coefficient, p: p-value).

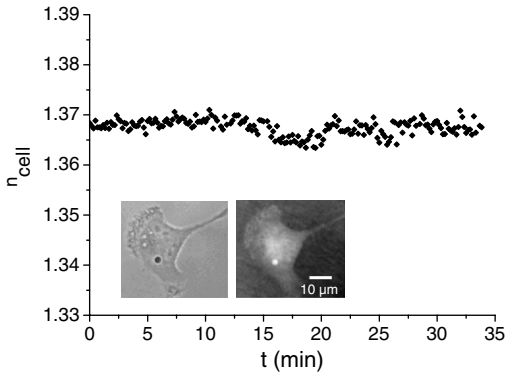

Fig. 4 Temporal dependency of the cellular refractive index n_{cell} under static conditions (evaluation of $N = 200$ digital holograms, $\Delta t = 10$ s, 320 mOsmol/kg); the inserts show a white light image (left panel) and a DHM phase image (right panel) of the investigated cell with an incorporated microsphere.

In a further experiment, n_{cell} was determined with two microparticles that were incorporated in a single cell. Figure 2(b) shows a representative white light image (left) and quantitative DHM phase images for 320 and 160 mOsmol/kg (middle and right, respectively). The microparticles labeled 4 and 5 were used to detect the intracellular refractive index; resulting refractive index values are plotted in Fig. 2(d). In analogy to the results in Fig. 2(c), the dependency from the osmolality is almost linear ($R \geq 0.988$, $p < 0.0001$). The comparison of the data from microspheres 4 and 5 in the right panel of Fig. 2(d) shows only small differences ($\Delta n_{cell} = 0.001$), and thus demonstrates the reliability of the refractive index determination procedure.

Figure 2(e) depicts the mean values $\bar{n}_{cell}$ obtained from the plots of all five microspheres in Fig. 2(c) and 2(d). The measurement uncertainty is obtained by calculation of the standard deviation. A highly linear dependency between $\bar{n}_{cell}$ and the osmolality is found ($R = 0.988$, $p < 0.0001$).

3.4 *Verification of the Cytoplasm Refractive Index Determination*

In order to verify the results in Sec. 3.3 for the cellular refractive index of adherent PaTu 8988 T cells with irregular shape, the method for refractive index determination was also applied to suspended PaTu 8988 T cells with incorporated microspheres. The morphology of detached cells in suspension typically changes to a spherical shape. Thus, the two-dimensional fitting procedure for refractive index determination of spherical objects described in Sec. 2.4 can be also used for comparative investigations on whole cells.[30] First, the refractive index of selected cells was analyzed with internalized microspheres in dependence of the osmolality of the cell culture medium in analogy to the experiments with adherent cells that are described in Sec. 3.3. Then, in comparison, the integral cellular refractive index was determined by fitting Eq. (3) to whole cells without incorporated microspheres. For each osmolality, $N = 25$ suspended cells with and without internalized microspheres were investigated [for illustration see quantitative phase image in Fig. 1(h)].

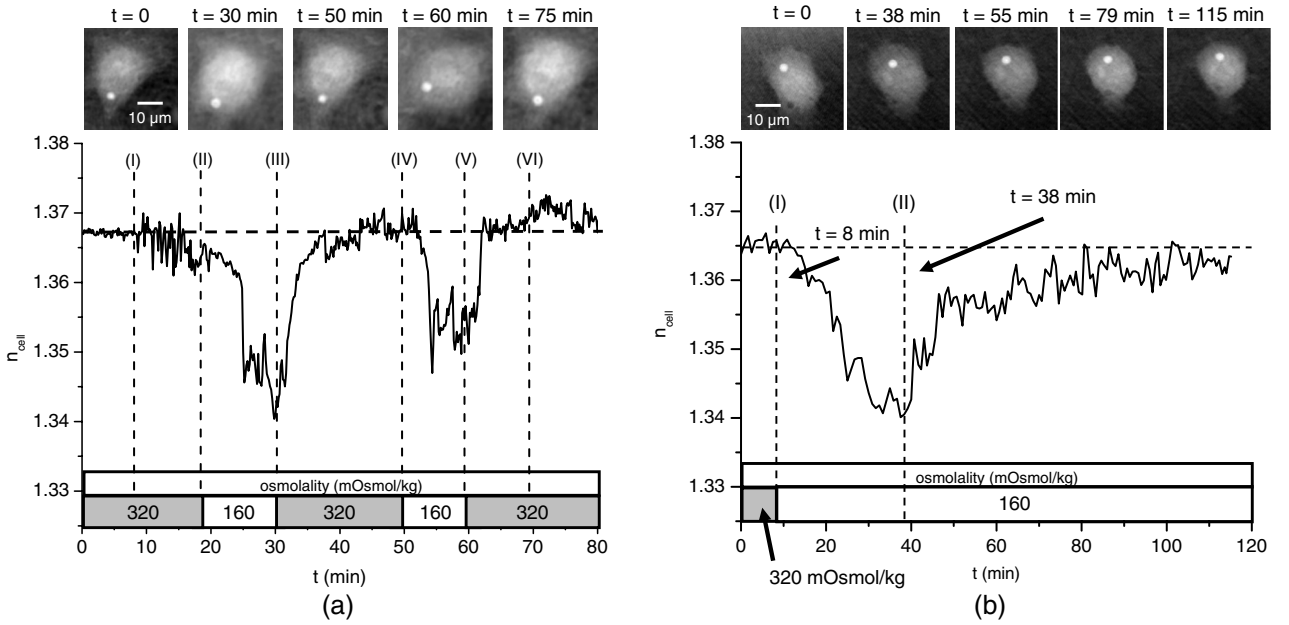

Fig. 5 (a) Temporal response of the cellular refractive index n_{cell} to repeated osmotic stimulation (evaluation of $N = 485$ digital holograms, $\Delta t = 10$ s); upper panel: representative quantitative DHM phase images of a HT-1080 cell with an incorporated microsphere at indicated time; lower panel: temporal dependency of n_{cell}; the pump system is started at $t = 8$ min (i) with a continuous flow rate of 1.99 ml/ min; at $t = 18$ min (ii) the osmolality of the cell culture medium is decreased from 320 to 160 mOsmol/kg; at $t = 30$ min (iii) the osmolality is increased to the initial value; at $t = 49$ min (iv) the osmolality is decreased again to 160 mOsmol/kg, at $t = 57$ min (v) the osmolality is increased to 320 mOsmol/kg; the pump system is stopped at $t = 80$ min (iv). (b) Temporal response of the cellular refractive index n_{cell} to a single osmotic stimulation (evaluation of $N = 180$ digital holograms, $\Delta t = 40$ s); upper panel: representative quantitative DHM phase images of a HT-1080 cell with an incorporated microsphere at indicated time; lower panel: temporal dependency of n_{cell}; the pump system is started at $t = 0$ with a continuous flow rate of 1.99 ml/ min; at $t = 8$ min (i) the osmolality of the cell culture medium is decreased from 320 to 160 mOsmol/kg; at $t = 38$ min (ii) the flow is stopped.

Figure 3(a) depicts the mean refractive index $\bar{n}_{cell}$ obtained with the internalized microspheres as a reference, while the corresponding values from the analysis of the whole cells in dependence of the osmolality are shown in Fig. 3(b). In Fig. 3(c), the data in Fig. 3(a) and 3(b) are compared. The intracellular refractive index obtained from the internalized particles increases linearly from $\bar{n}_{cell}(160\ \text{mOsmol/kg}) = 1.36 \pm 0.01$ to $\bar{n}_{cell}(320\ \text{mOsmol/kg}) = 1.38 \pm 0.02$ ($R = 0.986$, $p < 0.0001$). The same tendency is found in Fig. 3(b), where the corresponding refractive index data of the whole cells are plotted. In this case, the refractive index increases from an initial value $\bar{n}_{cell}(160\ \text{mOsmol/kg}) = 1.356 \pm 0.003$ to $\bar{n}_{cell}(320\ \text{mOsmol/kg}) = 1.373 \pm 0.004$ ($R = 0.990$, $p < 0.0001$).

The measurement uncertainty for the whole cells [Fig. 3(b)] is lower than the microspheres [Fig. 3(a)]. This is plausible as the area in the DHM image includes more phase values for the determination of n_{cell} in the whole cell. However, the comparison in Fig. 3(c) shows that for all osmolalities, the refractive indices of the whole cells are slightly lower than the microspheres. This may be explained by the circumstance that the particles are located within the cytoplasm, while the refractive index of the whole cells also includes the refractive index of the nucleus, which has been reported in some cases to have a slightly lower refractive index than the cytoplasm.[23] Nevertheless, within the measurement uncertainty, the obtained refractive index values from the suspended cells in Fig. 3 are found in good agreement with the data in Fig. 2, and thus validate the procedure for refractive index determination of adherent cells with internalized microspheres.

3.5 *Analysis of Dynamic Refractive Index Changes in Adherent Cells*

Investigations on the reproducibility of refractive index sensing with internalized microspheres in adherent cells are performed with self-interference DHM using the microfluidics chamber and the pump system. In a first experiment, a HT-1080 cell with an incorporated microsphere is observed for 35 min in an isotonic cell culture medium (320 mOsmol/kg) under static conditions; $N = 200$ digital self-interference holograms were recorded every 10 s and evaluated as described in Secs. 2.3 and 2.4. Figure 4 shows the resulting temporal dependency of the cellular refractive index, as well as representative white light and quantitative DHM phase images of the investigated cell. For the whole measurement period, only few fluctuations of n_{cell} are observed. The mean refractive index and its standard deviation are determined as $\bar{n}_{cell} = 1.368 \pm 0.002$.

In a second experiment, another cell is exposed after $t = 8$ min under static conditions, and for 10 min after exposure to a continuous flow (flow rate 1.99 ml/min). At $t = 18$ min, the osmolality is changed with the pump system to 160 mOsmol/kg. After 12 min more, the osmolality is changed again to 320 mOsmol/kg. At $t = 49$ min, the procedure is repeated. During the experiment, $N = 485$ digital holograms are recorded ($\Delta t = 10$ s) and are evaluated in analogy to Fig. 4.

Figure 5(a) depicts the results. In the phase maps in the upper panel of Fig. 5(a), cell swelling and shrinking due to the osmolality changes is observed. In the lower panel of Fig. 5(a), for each osmolality change, the cellular refractive index n_{cell} decreases and increases in a similar range as for the values that are obtained for the PaTu 8988 T cells (see Secs. 3.3 and 3.4). For each period of the experiment, the sensitivity for detection of refractive index changes is quantified by the calculation of the standard deviation of the temporal fluctuations of n_{cell}. Without flow, in the period from $t = 0$ to 8 min, the standard deviation of n_{cell} amounts to 0.001. After the start of the continuous flow from $t = 8$ to 18 min, the standard deviation of n_{cell} increases significantly to 0.007. This may be explained by rearrangement activities of the cell as a response to the flow. For all other periods from $t = 18$ to 80 min, the refractive index fluctuations are found in the range from 0.002 to 0.006. These fluctuations may be induced by cell movements and motions of the microsphere inside the cell during the measurements as well as by an enhanced phase noise due to flow and diffraction patterns of moving dust particles inside the cell culture medium.

In a final series of experiments, we explored if the sensitivity of the method was sufficient to detect refractive index changes related to cellular volume regulation processes. Therefore, the response of the cellular refractive index is measured under the same flow conditions as in the previous experiment; however, in contrast to Fig. 5(a), only a single change of the osmolality of the cell culture medium was performed. Digital holograms were recorded every 40 s. At $t = 0$ the flow was

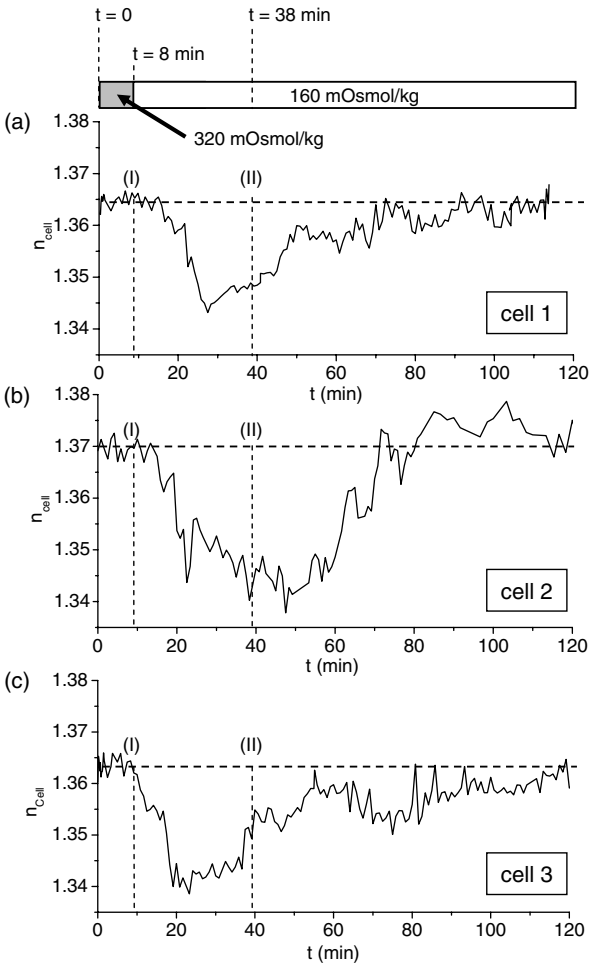

Fig. 6 Temporal response of the refractive indices n_{cell} of three different HT-1080 cells to a single osmotic stimulation. (a) cell 1 (b) cell 2 (c) cell 3. For each measurement $N = 180$ digital holograms were recorded ($\Delta t = 40$ s). The measurements started at $t = 0$ with a continuous flow rate of 1.99 ml/min; at $t = 8$ min (i) the osmolality of the cell culture medium was decreased from 320 to 160 mOsmol/kg; at $t = 38$ min (ii) the flow is stopped.

started, and at $t = 8$ min, the osmolality was changed to 160 mOsmol/kg. At $t = 38$ min the flow was stopped and the cell was further observed until $t = 120$ min.

Figure 5(b) shows representative DHM phase contrast images and the resulting temporal dependency of n_{cell}. Similarly to Fig. 5(a), swelling and slight detachment of the cell is observed until $t \approx 38$ min [upper panel of Fig. 5(b)]; however, for $t > 40$ min the cell starts to shrink again. The shrinking process is accompanied with an increase of n_{cell} that is detected with the microsphere. At $t = 120$ min, the cell has nearly recovered its initial refractive index completely, and other than a slight detachment due to the swelling process, no significant morphology changes are observed in the DHM phase images. In order to study the effect that is shown in Fig. 5(b) more precisely, three additional cells were investigated in three independently performed measurements. Figure 6 shows the obtained temporal refractive index dependencies. Although no uniform response of the cells to the osmotic stimulation was observed, all cells reach within the uncertainty range of the measurement their initial refractive index values. The increase of the refractive index after the decrease of the osmolality may be explained by regularly volume decrease processes.[44]

4 Conclusions

A method in which silica microspheres are used as a reference in quantitative phase images to determine the refractive index of living adherent cells was presented. In preliminary investigations, it was shown that quantitative phase imaging represents a versatile label-free method to determine the size and refractive index of microspheres in different solvents. Furthermore, DHM phase contrast is a helpful tool for verifying if microparticles are internalized by a living cellular specimen. Experiments on osmotically stimulated adherent human pancreatic tumor cells and fibro sarcoma cells were performed to characterize the method and its usage in combination with microfluidics. The results demonstrate that internalized microspheres can be used as probes in adherent cells to determine the refractive index of the cytoplasm. Furthermore, the results in Sec. 3.5 show the method can be applied for refractive index sensing of adherent cells in continuous flow. The experimentally obtained refractive index values are found in good agreement with previously published data for the cellular refractive index.[20,23,31,34] The absolute accuracy for refractive index determination with microspheres in comparison to adherent and suspended cells is lower as if whole suspended cells with spherical shape are considered (see Secs. 3.4 and 3.5). However, a relative sensitivity for temporal refractive index changes up to 0.001 is achieved. This can be explained by fixed coherence induced parasitic interferences and scattering patterns. Such static patterns lead to a local increase of the spatial phase noise, but do not affect the sensitivity for the detection of time dependent relative phase changes. From the results in Sec. 3.5, it can be concluded that our approach may lead to a higher precision in the analysis of the water permeability of the cell membrane.[45,46] The high sensitivity for the detection of relative refractive index changes may also be sufficient for the analysis of concentration changes of intracellular solutes due to cell volume regulation processes.[44] Furthermore, the method may be applied to adherent cells for detection of dynamic intracellular solute concentration changes in neurophysiology[47] in the analysis of toxin-mediated cell alterations[48] and early cell death detection,[49] or during stem cell differentiation,[50] infection processes,[51] and laser photoporation,[52] however, this requires further systematic investigations with suitable cell models.

As no modification of the experimental setup is required, the measurement principle prospects to be used with several existing quantitative phase contrast imaging techniques,[1–16] and the usage in multi-modal imaging platforms[53] is simplified. Finally, as many cells internalize particles by phagocytic behavior, the method may be applicable with a variety of different cell types. In conclusion, the method prospects to be a useful tool in quantitative phase microscopy-based live cell imaging of adherent cells to enhance the precision for morphology measurements, and for the quantification of intracellular solute concentration changes.

Acknowledgments

This work was partly supported by the German Federal Ministry for Education and Research within the focus program "Biophotonics" (FKZ 13N10937). Furthermore, the authors thank Christina Rommel and Jürgen Schnekenburger from the Biomedical Technologies Center, Medical Faculty of the University of Muenster, Germany, for the support with the pancreatic tumor cells.

References

1. A. Barty et al., "Quantitative optical phase microscopy," *Opt. Lett.* **23**(11), 817–819 (1998).
2. E. Cuche, P. Marquet, and C. Depeursinge, "Simultaneous amplitude-contrast and quantitative phase-contrast microscopy by numerical reconstruction of fresnel off-axis holograms," *Appl. Opt.* **38**(34), 6694–7001 (1999).
3. V. P. Tychinskii, "Coherent phase microscopy of intracellular processes," *Phys. Usp.* **44**(6), 617–629 (2001).
4. D. Carl et al., "Parameter-optimized digital holographic microscope for high-resolution living-cell analysis," *Appl. Opt.* **43**(3), 6536–6544 (2004).
5. C. J. Mann et al., "High-resolution quantitative phase-contrast microscopy by digital holography," *Opt. Express* **13**(22), 8693–8698 (2005).
6. T. Ikeda et al., "Hilbert phase microscopy for investigating fast dynamics in transparent systems," *Opt. Lett.* **30**(10), 1165–1167 (2005).
7. P. Marquet et al., "Digital holographic microscopy: a noninvasive contrast imaging technique allowing quantitative visualization of living cells with subwavelength axial accuracy," *Opt. Lett.* **30**(5), 468–470 (2005).
8. G. Popescu et al., "Diffraction phase microscopy for quantifying cell structure and dynamics," *Opt. Lett.* **31**(6), 775–778 (2006).
9. C. Joo et al., "Spectral-domain optical coherence phase and multiphoton microscopy," *Opt. Lett.* **32**(6), 623–625 (2007).
10. P. Bon et al., "Quadriwave lateral shearing interferometry for quantitative phase microscopy of living cells," *Opt. Express* **17**(15), 13080–13094 (2009).
11. N. T. Shaked et al., "Whole-cell-analysis of live cardiomyocytes using wide-field interferometric phase microscopy," *Biomed. Opt. Express* **1**(2), 706–719 (2010).
12. H. Ding and G. Popescu, "Instantaneous spatial light interference microscopy," *Opt. Express* **18**(2), 1569–1575 (2010).
13. L. Waller et al., "Phase from chromatic aberrations," *Opt. Express* **18**(22), 22817–22825 (2010).
14. J. Frank et al., "Refractive index determination of transparent samples by noniterative phase retrieval," *Appl. Opt.* **50**(4), 427–433 (2011).
15. S. S. Kou et al., "Transport-of-intensity approach to differential interference contrast (TI-DIC) microscopy for quantitative phase imaging," *Opt. Lett.* **35**(3), 447–449 (2010).
16. M. Rinehart, Y. Zhu, and A. Wax, "Quantitative phase spectroscopy," *Biomed. Opt. Express* **3**(5), 958–965 (2012).
17. B. Kemper et al., "Investigation of living pancreas tumor cells by digital holographic microscopy," *J. Biomed. Opt.* **11**(4), 034005 (2006).
18. Y. Jang, J. Jang, and Y. K. Park, "Dynamic spectroscopic phase microscopy for quantifying hemoglobin concentration and dynamic membrane fluctuations in red blood cells," *Opt. Express* **20**(9), 9673–9681 (2012).

19. Y. K. Park et al., "Spectroscopic phase microscopy for quantifying hemoglobin concentrations in intact red blood cells," *Opt. Lett.* **34**(23), 3668–3670 (2009).
20. B. Rappaz et al., "Measurement of the integral refractive index and dynamic cell morphotometry of living cells with digital holographic microscopy," *Opt. Express* **13**(23), 9361–9373 (2005).
21. G. Popescu et al., "Optical imaging of cell mass and growth dynamics," *Am. J. Physiol. Cell Physiol.* **295**(2), C538–C544 (2008).
22. V. Lauer, "New approach to optical diffraction tomography yielding a vector equation of diffractive tomography and a novel tomographic microscope," *J. Microsc.* **205**(2), 165–176 (2002).
23. W. Choi et al., "Tomographic phase microscopy," *Nature Methods* **4**, 717–719 (2007).
24. M. Debailleul et al., "High-resolution threedimensional tomographic diffractive microscopy of transparent inorganic and biological samples," *Opt. Lett.* **34**(1), 79–81 (2009).
25. R. Barer, "Refractometry and interferometry of living cells," *J. Opt. Soc. Am.* **47**(6), 545–556 (1957).
26. T. Fukano and I. Yamaguchi, "Separation of measurement of the refractive index and the geometrical thickness by use of a wavelength-scanning interferometer with a confocal microscope," *Appl. Opt.* **38**(19), 4065–4073 (1999).
27. W. Z. Song et al., "Refractive index measurement of single living cells using on-chip Fabry-Pérot cavity," *Appl. Phys. Lett.* **89**(20), 203901 (2006).
28. C. L. Curl et al., "Refractive index measurement in viable cells using quantitative phase-amplitude microscopy and confocal microscopy," *Cytometry Part A* **65**(1), 88–92 (2005).
29. N. Lue et al., "Live cell refractometry using microfluidic devices," *Opt. Lett.* **31**(18), 2759–2761 (2006).
30. S. Kosmeier et al., "Determination of the integral refractive index of cells in suspension by digital holographic phase contrast microscopy," *Proc. SPIE* **6991**, 699110 (2008).
31. B. Kemper et al., "Integral refractive index determination of living suspension cells by multifocus digital holographic phase contrast microscopy," *J. Biomed. Opt.* **12**(5), 054009 (2007).
32. M. Kemmler et al., "Noninvasive timedependent cytometry monitoring by digital holography," *J. Biomed. Opt.* **12**(6), 064002 (2007).
33. F. E. Robles, L. L. Satterwhite, and A. Wax, "Nonlinear phase dispersion spectroscopy," *Opt. Lett.* **36**(23), 4665–4667 (2011).
34. B. Rappaz et al., "Simultaneous cell morphometry and refractive index measurement with dual-wavelength digital holographic microscopy and dye-enhanced dispersion of perfusion medium," *Opt. Lett.* **33**(7), 744–746 (2008).
35. F. Charrière et al., "Cell refractive index tomography by digital holographic microscopy," *Opt. Lett.* **31**(2), 178–180 (2006).
36. F. Charrière et al., "Living specimen tomography by digital holographic microscopy: morphometry of testate amoeba," *Opt. Express* **14**(16), 7005–7013 (2006).
37. P. Mthunzi et al., "Intracellular dielectric tagging for improved optical manipulation of mammalian cells," *IEEE J. Quan. Electron.* **16**(3), 608–618 (2010).
38. H. P. Elsässer et al., "Establishment and characterisation of two cell lines with different grade of differentiation derived from one primary human pancreatic adenocarcinoma," *Virchows Arch. B Cell Pathol. Mol. Pathol.* **61**(1), 295–306 (1992).
39. S. Rasheed, W. A. Nelson Rees, and E. M. Toth, "Characterization of a newly derived human sarcoma cell line (HT 1080)," *Cancer* **33**(4), 1027–1033 (1974).
40. E. Erba et al., "Cell kinetics of human ovarian cancer with in vivo administration of bromodeoxyuridine," *Ann. Oncol.* **5**(7), 627–634 (1994).
41. B. Kemper et al., "Modular digital holographic microscopy system for marker free quantitative phase contrast imaging of living cells," *Proc. SPIE* **6191**, 61910T (2006).
42. B. Kemper et al., "Simplified approach for quantitative digital holographic quantitative phase contrast imaging of living cells," *J. Biomed. Opt.* **16**(2), 026014 (2011).
43. P. Langehanenberg et al., "Autofocusing in digital holographic phase contrast microscopy on pure phase objects for live cell imaging," *Appl. Opt.* **47**(19), D176–D182 (2008).
44. E. K. Hoffmann, O. H. Lambert, and S. F. Pedersen, "Physiology of cell volume regulation in vertebrates," *Physiol. Rev.* **89**(1), 193–277 (2009).
45. J. Farinas and A. S. Verkman, "Cell volume and plasma membrane osmotic water permeability in epithelial cell layers measured by interferometry," *Biophys. J.* **71**(6), 3511–3522 (1996).
46. J. Klokkers et al., "Atrial natriuretic peptide and nitric oxide signaling antagonizes vasopressin-mediated water permeability in inner medullary collecting duct cells," *Am. J. Physiol. Renal Physiol.* **297**(3), F693–F703 (2009).
47. P. Jourdain et al., "Determination of transmembrane water fluxes in neurons elicited by glutamate ionotropic receptors and by the cotransporters KCC2 and NKCC1: a digital holographic microscopy study," *J. Neurosci.* **31**(33), 11846–11854 (2011).
48. A. Bauwens et al., "Differential cytotoxic actions of Shiga toxin 1 and 1 Shiga toxin 2 on microvascular and macrovascular endothelial cells," *Thrombosis and Haemostasis* **105**(3), 515–528 (2011).
49. N. Pavillon et al., "Early cell death detection with digital holographic microscopy," *PLos ONE* **7**(1), e30912 (2012).
50. K. J. Chalut et al., "Quantifying cellular differentiation by physical phenotype using digital holographic microscopy," *Integr. Biol.* **4**(3), 280–284 (2012).
51. Y. K. Park et al., "Refractive index maps and membrane dynamics of human red blood cells parasitized by Plasmodium falciparum," *PNAS* **105**(37), 13730–13735 (2008).
52. M. Antkowiak et al., "Quantitative phase study of the dynamic cellular response in femtosecond laser photoporation," *Biomed. Opt. Express* **1**(2), 414–424 (2010).
53. M. Esseling et al., "Multimodal biophotonic workstation for live cell analysis," *J. Biophoton.* **5**(1), 9–13 (2012).